**Corrosion behavior of CoCrNi medium-entropy alloy compared with 304 stainless steel in $H_2SO_4$ and NaOH solutions**

Jianying Wang[1], Wenhao Li[1], Hailin Yang[1]*, Zhilin Liu[3], Hua Huang[1], Shouxun Ji[2], Jianming Ruan[1]

1. State Key Laboratory of Powder Metallurgy, Central South University, Changsha 410083, China

2. BCAST, Brunel University London, Uxbridge, Middlesex, UB8 3PH, United Kingdom

3. College of Mechanical and Electrical Engineering, Central South University, Changsha, 410083, China

*Corresponding authors: Hailin Yang, y-hailin@csu.edu.cn

**Abstract**

The corrosion resistance and passive film properties of the CoCrNi medium-entropy alloy were investigated. The results show that selective dissolution of elements in the CoCrNi is evident compared with the 304 SS. The passive film formed on the CoCrNi is enriched in Cr but depleted in Co and Ni，and the high content of Cr and thicker passive film are responsible for the higher anti-corrosion of the CoCrNi in $H_2SO_4$ solution; the surface is enriched in Co but depleted in Cr and Ni, and the higher dissolution rate of Cr is responsible for the lower anti-corrosion in NaOH solution.

***Keywords**:* A. Alloy; B. Polarization, XPS; C. Acid corrosion; C. Alkaline corrosion

## 1. Introduction

The entropy-based alloys， in particular for high- and medium-entropy alloys (HEAs/MEAs), shape an entirely new field of alloy design and attract increasing significant attention in the community of materials science community [1-4]. Much of the interest stems from the belief that new alloy systems with superior properties are likely to be found near the centres (rather than corners) of phase diagrams in compositionally complex systems [5]. Particularly, medium-entropy alloys consisting of two to four principal elements are a newly emerging class of materials with superior mechanical response [6–9]. Accordingly, various MEA systems have been designed and fabricated during the past years, such as face-centered cubic (fcc) CoCrNi [7-9] and body-centered cubic (bcc) TiZrNbTa [10-12]. Among these, the CoCrNi MEA which was first reported by Wu et al. [13], has particularly excellent mechanical properties at cryogenic and room temperature than typical CoCrFeMnNi HEA and most multi-phase alloys [3].

Currently, the corrosion behavior of some types of HEAs and MEAs in various aqueous solutions has been investigated. Luo et al. [14] studied the corrosion resistance and passive film properties of the CoCrFeMnNi compared with the 304L SS in 0.1 M $H_2SO_4$ solution. The results indicate that the lower anti-corrosion performance is ascribed to low content of Cr and the extensive formation of metal hydroxide in the passive film. In addition, the increasing Al content of the $Al_xCoCrFeNi$ in a 3.5 wt.% NaCl solution leads to thicker/dispersive passive films that degrade the localized corrosion resistance [15]. Moreover, Niu et al. revealed that the $Al_{0.5}FeCoCrNiCu$ shows preferable corrosion and pitting resistance in 0.5 M $H_2SO_4$ and 1 M NaCl solutions compared with the 304L SS [16]. More recently, Feng et al. [17] investigated the corrosion behavior of the high nitrogen CrCoNiN in 3.5 wt.% NaCl solution, lower metastable pitting susceptibility together with compact passive film are responsible for the improvement of corrosion resistance in counterpart with the CoCrNi. Besides, the CoCrFeNi has markedly superior pitting resistance than the 304L SS in 3.5 wt.% NaCl solution, owing to its high Cr content [18]. Also, the large potential difference between metal matrix and Cu-rich solid solution deteriorates the corrosion resistance of the $CoCrFeNiCu_x$ coatings in 3.5 wt.% NaCl solution [19].

As described earlier, the CoCrNi exhibits outstanding mechanical response at cryogenic and room temperature than the CoCrFeMnNi and most multi-phase alloys

[3]. However, without satisfactory corrosion resistance, these HEAs/MEAs with outstanding mechanical properties are not enough for long-term engineering applications. Compared with the CoCrFeMnNi and the 304 SS, the CoCrNi might possess preferable corrosion resistance due to the higher concentration of passivating elements, such as Cr and Ni, which facilitate the formation of protective passive layers. In addition, these three kinds of alloys have a single-phase fcc structure with similar lattice parameter (~0.36 nm [20,21]). Although Feng et al. [17] has investigated the corrosion resistance of the CoCrNi and the CoCrNiN in 3.5 wt.% NaCl solution, detailed information, such as the corrosion mechanisms in acid and alkali solutions, are still unknown and it is of interest to understand whether the corrosion resistance of the CoCrNi with higher atomic ratio of Cr and Ni is superior than the well-established 304 SS.

Motivated by the above considerations, in this work, the corrosion behavior of the CoCrNi compared with the 304 SS in 1 M $H_2SO_4$ and 1.5 M NaOH solutions was investigated. The passivation behavior and composition of the passive film of the CoCrNi and the 304 SS were investigated by electrochemical impedance spectroscopy (EIS) and X-ray photoelectron spectroscopy (XPS), respectively. The surface morphologies of samples after test were measured using scanning electron microscope (SEM). The concentrations of elements in the corrosive solutions before and after exposure were determined using the inductively coupled plasma method (ICP). Our main aim is to identify the corrosion mechanism of the CoCrNi.

## 2. Experimental

### 2.1 Materials preparation

Co, Cr and Ni ingots with high purity (99.95 wt.%) were used as raw materials. The CoCrNi was fabricated by high-pressure nitrogen gas atomization and spark plasma sintering (SPS) methods. The ingots were heated up to the operating temperature (Tm = 1943 K) and the molten alloy was ejected through a nozzle with a $N_2$ pressure of 1.8 MPa. The CoCrNi gas atomization powder was subsequently consolidated by SPS in a 40 mm-inner-diameter graphite die at 1473 K for 15 min. A commercial compositions 304 SS sheet with a thickness of 5 mm was used as reference material. Samples with dimensions 10 mm × 10 mm × 2 mm were machined from the alloy sheets. The electrodes used for the electrochemical tests were connected by a wire

welded to the back side of the samples, and sealed with a curing epoxy resin, leaving only one face with a size of 1 $cm^2$ exposed to the solution. 1 M $H_2SO_4$ and 1.5 M NaOH solutions were used as electrolyte during the testing.

### 2.2 Microstructural analysis

X-ray diffraction (XRD, Rigaku X-2000) was utilized to characterize the phase structure. A scanning electron microscope (SEM, FEI nano 230 field emission) equipped with an energy-dispersive spectrometer (EDS) was used to observe microstructures and phase compositions. Electron backscatter diffraction (EBSD) measurements were carried out using a FIB Helios NanoLab G3 UC scanning electron microscope (SEM) with a Hikari camera and the TSL OIM data collection software.

### 2.3 Electrochemical performance tests

The samples were washed by deionized water and anhydrous ethanol with an ultrasonic cleaner and then dried in air at room temperature. The electrochemical test was conducted with a multichannel electrochemical workstation (CHI 660). Saturated calomel electrode (SCE) and platinum were used as the reference electrode and auxiliary electrode, respectively. In addition, a salt bridge carried by polytetrafluoroethylene was arranged to reduce the liquid junction potential and protect the reference electrode. Corrosion resistance was evaluated by Tafel method and electrochemical impedance spectroscopic (EIS). The concentrations of various metal ions in test solution after polarization were determined by inductively coupled plasma (ICAP 7600 SERIES). Before the test, samples were immersed in test solutions for 1 h to make the samples reach a stable state. Every test was performed for at least 5 times to guarantee the satisfactory reproducibility.

### 2.4 Characterization of the passive films

To investigate the influence of the passive films on the alloys, the samples were polarized at +500 mV for 5 min to get the passive films formed. The composition of the passive films was determined by the X-ray photoelectron spectroscopy (ESCALAB 250Xi) and sputtering technology was carried out to obtain depth profiles of the different elements. The XPS data were analyzed using software Thermo Avantage (version 5.52). The surface morphology and the distribution of the various elements of the alloys after polarization were detected by field emission scanning electron microscope (FEI nano 230 field emission) and EDS mapping.

## 3. Results and discussion

### 3.1 Starting microstructure

SEM and EBSD images taken from the sheets reveal that both types of materials exhibit recrystallized microstructure with a trace of twins. The XRD patterns inserted in Fig. 1d confirm the fcc structure with similar lattice parameters in both materials. The average grain sizes of the CoCrNi and the 304 SS are ~21 μm and 11 μm, respectively. Previous studies have shown that only nanoscale grain size has obvious effect on the corrosion of stainless steel. This is due to the increasing diffusion rates along interfaces, which enables the elements to migrate faster and form a protective passive film in nano-grained materials [22-25]. Thus, the difference in grain size between the two kinds of alloys does not affect the results of this study.

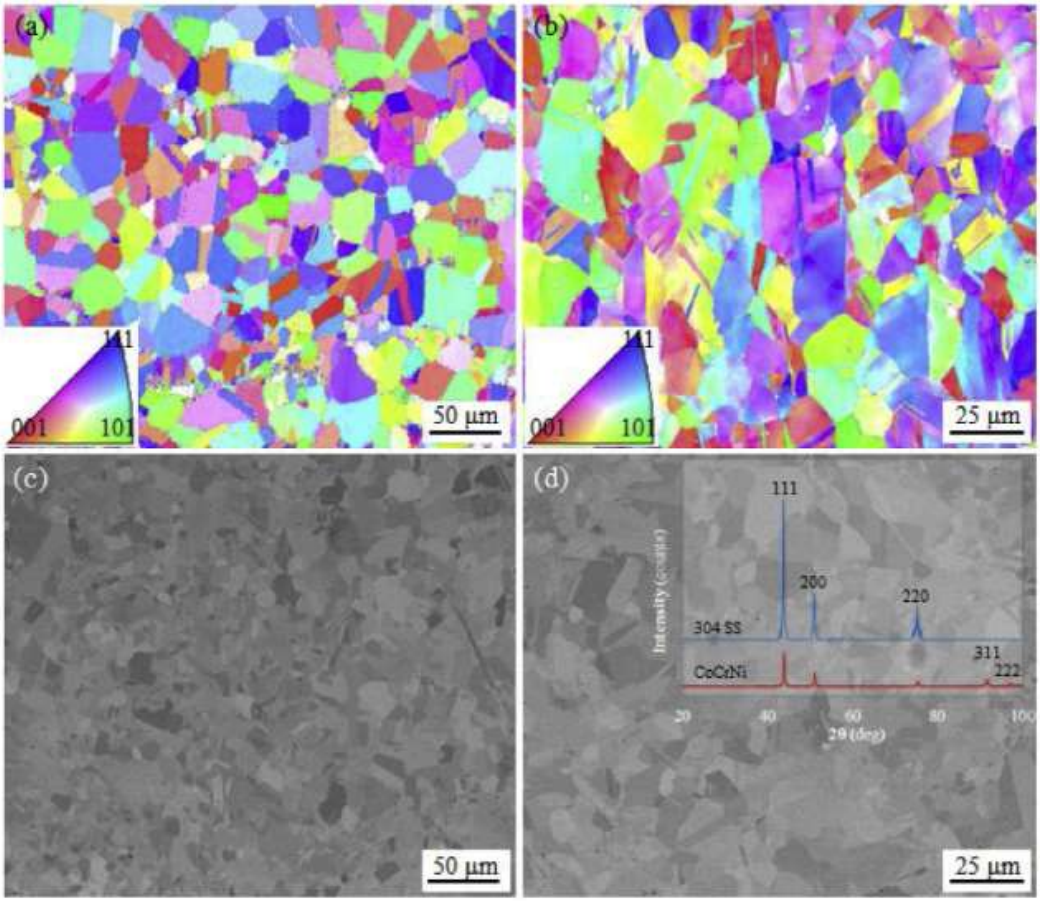


Fig. 1.Starting microstructures of (a) (c) the CoCrNi and (b) (d) the 304 SS samples prior to corrosion testing. The inset in (d) shows the XRD patterns of the two alloys.

### 3.2 Electrochemical corrosion behavior and element-resolved analysis

Fig. 2 shows the typical polarization curves for the CoCrNi and the 304 SS in 1 M $H_2SO_4$ and 1.5 M NaOH solutions at room temperature. It can be seen that the CoCrNi and the 304 SS exhibit similar features with a passive potential range extending from the corrosion potential to the onset of transpassivity in $H_2SO_4$ solution. In NaOH solution, the 304 SS shows passive behavior while CoCrNi does not. Moreover, the anodic current of the 304 SS is lower than that of the CoCrNi, indicating that the 304 SS has lower dissolution rate than the CoCrNi.

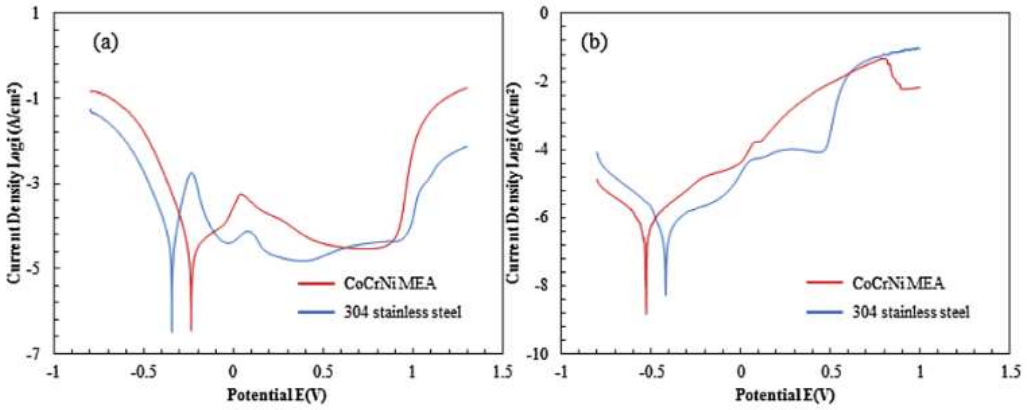


Fig. 2. Potentiodynamic polarization curves of the CoCrNi and the 304 SS in H2SO4 solution (a) and NaOH solution (b) at room temperature

**Table 1**
Compositions of the CoCrNi MEA and the 304 SS according to wet-chemical analysis (wt.%).

| Materials | C | Cr | Ni | P | S | Si | Co | Mn | Fe |
|---|---|---|---|---|---|---|---|---|---|
| CoCrNi | - | 31.6 % | 33.9 % | - | - | - | 34.5 % | - | - |
| 304 SS | 0.029 % | 8.93 % | 18.56 % | 0.017 % | 0.014 % | 0.15 % | - | 0.89 % | 71.41 % |

Table 1 summarizes some of the associated corrosion electrochemical parameters obtained by fitting the polarization data, such as the corrosion potential ($E_{corr}$), the cathodic ($\beta c$), anodic ($\beta a$) slops and the polarization resistance ($R$). Corrosion current density ($J_{corr}$) is a parameter which is widely used to evaluate the corrosion resistance of materials [26,27]. Usually, lower value of it can be considered to be a sign that the material shows fine corrosion resistance. From the Table 1, it is obvious that the $J_{corr}$ of the CoCrNi is lower than that of the 304 SS in 1 M $H_2SO_4$ solution, which means that the CoCrNi exhibits superior corrosion resistance in $H_2SO_4$ solution. However,

the higher $J_{corr}$ of the 304 SS in 1.5 M NaOH solution suggests that the 304 SS shows preferable corrosion resistance than the CoCrNi. $R$ is associated with the ability of materials to prevent corrosion occurring, and larger value of it means the barrier to corrosion is higher [28,29]. Obviously, The $R$ of the CoCrNi is higher than that of the 304 SS in $H_2SO_4$ solution but opposite in NaOH solution, which confirms the aforementioned conclusions.

To better understand the corrosion process of the CoCrNi and the 304 SS in two kinds of solutions, ICP was carried out to determine the concentrations of metal ions in solutions after the Tafel test. The results are presented in Table 2. In 1 M $H_2SO_4$ solution, the 304 SS shows a high dissolution rate of Fe according to the fact the concentration of Fe ions (14.00 mg/L) exceeds that of the other metal ions. In addition, the concentration of Cr ions (653. 42 μg/L) is lower than that of Co ions (3241.66 μg/L) and Ni ions (5946.20 μg/L) due to the formation of a Cr-oxides passive film. Cr-oxides passive film on stainless steel is ascribed to the selective dissolution of Fe passivation, leaving Cr enriched in the passive film [30-33]. In terms of the CoCrNi in $H_2SO_4$ solution, similar to the 304 SS, selective dissolution also occurred on the surface of alloy and the concentration of Cr ions (3929.64 μg/L) are significantly lower than the concentrations of Co ions (20557.69 μg/L) and Ni ions (23337.93 μg/L). One of the main reasons why the concentrations of dissolved Co, Cr and Ni ions in the case of the CoCrNi are higher than the 304 SS is that the raw fractions of the CoCrNi are much higher than that of the 304 SS.

**Table 2**
The electrochemical parameters estimated from polarization data for the CoCrNi and 304 SS in $H_2SO_4$ and NaOH solutions.

| Samples | $\beta a$ (V per decade) | $\beta c$ (V per decade) | $i_{corr}$ (μA $cm^{-2}$) | $E_{corr}$ (V) | $R(\Omega)$ |
|---|---|---|---|---|---|
| 304 SS ($H_2SO_4$) | 16.67 | −10.53 | 46.10 | −0.34 | 403 |
| CoCrNi ($H_2SO_4$) | 3.42 | −11.64 | 32.40 | −0.24 | 848 |
| 304 SS (NaOH) | 4.46 | −7.29 | 0.46 | −.0.47 | 72,036 |
| CoCrNi (NaOH) | - | - | - | - | - |

In terms of the 304 SS in 1.5 M NaOH solution, only a relatively small amount of Fe ions (~6.00 mg/L) and sub-stoichiometric concentrations of Cr ions (~1.82 μg/L) and Mn ions (~1.67 mg/L) dissolve in the solution, indicating that the 304 SS has superior corrosion resistance in NaOH solution. However, as for the CoCrNi in NaOH solution, much more Cr ions (~1913.71 μg/L) dissolves than Co ions (~50.26 μg/L) and Ni ions (~38.37 μg/L), which is the main reason why the 304 SS shows superior corrosion resistance than the CoCrNi in NaOH solution. From the above analysis, it is known that Cr element plays an important role in corrosion resistance in $H_2SO_4$ and NaOH solutions for both of the alloys. Such beneficial effect is weakened when it comes to 1.5 M NaOH solution for the CoCrNi.

### 3.3 Characteristics of the passive films

Electrochemical impedance spectroscopic (EIS) was carried out to understand the corrosion mechanism of the CoCrNi and the 304 SS in 1 M $H_2SO_4$ and 1.5 M NaOH solutions in the further. The Nyquist plots and Bode plots of the CoCrNi and the 304 SS in $H_2SO_4$ solution are illustrated in Fig. 3a and 3b. Only one capacitive loop is shown in the Nyquist plots of both of the alloys, which means that the corrosion reaction in $H_2SO_4$ solution is kinetically controlled by the process of charge transfer [34,35]. The conclusion can also be confirmed by the only peak in each Bode plot. The diameter of semi-arc in Nyquist plots reflects the corrosion resistance of the materials in solution [36]. The larger diameter of semi-arc of the Nyquist plots, the higher corrosion resistance of the passive film. Therefore, the Nyquist plots further confirm that the corrosion resistance of the CoCrNi is superior than the 304 SS in $H_2SO_4$ solution. In addition, the angle θ of Bode plot of the CoCrNi close to −80° in the intermediate range of frequency, suggesting that a stable passive film was formed in $H_2SO_4$ solution [37]. A relatively lower angle θ (∼−70°) of Bode plot of the 304 SS indicates that a unstable or non-dense passive film was formed in $H_2SO_4$ solution. In addition, the Nyquist plots and Bode plots of the CoCrNi and the 304 SS in NaOH solution are shown in Figs. 3c and 3d. Both the Nyquist plots exhibit incomplete capacitive loop and the diameter of semi-arc of the CoCrNi is smaller than that of the 304 SS. Besides, it should be noticed that the Bode plot of the CoCrNi shows two peaks while there is only one for the 304 SS. This means that the corrosion reaction of the CoCrNi in NaOH solution is affected by additional variable apart from applied

potential. The higher semi-arc of Nyquist plot, the peaks of Bode plot corresponding to lower frequency and higher angle confirm that the 304 SS has preferable corrosion resistance in NaOH solution further.

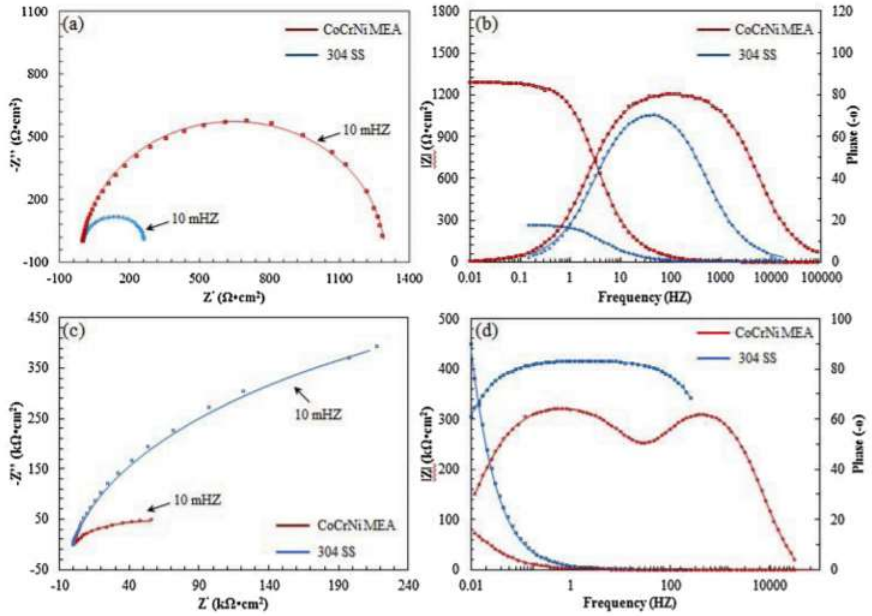


**Fig. 3.** Nyquist and Bode plots of the CoCrNi and the 304 SS after immersion in $H_2SO_4$ solution (a and b) and NaOH solution (c and d). (Note: the scattered symbols represent the experimental data and the solid lines represent the fitted results.).

**Table 3**
Concentrations of metal ions in test solutions after the Tafel test.

| Samples | Cr(μg/L) | | | Mn(μg/L) | | | Fe(mg/L) | | | Co(μg/L) | | | Ni(μg/L) | | |
|---|---|---|---|---|---|---|---|---|---|---|---|---|---|---|---|
| | OCP | Passive | Transpassive | OCP | Passive | Transpassive | OCP | Passive | Transpassive | OCP | Passive | Transpassive | OCP | Passive | Transpassive |
| 304 SS ($H_2SO_4$) | 0.71 | 0.11 | 652.60 | 0.05 | 0.01 | 0.12 | 4.82 | 0.01 | 9.17 | - | - | - | 80.50 | 10.80 | 5854.90 |
| CoCrNi ($H_2SO_4$) | 3.48 | 0.23 | 3925.93 | - | - | - | - | - | - | 323.50 | 74.20 | 20160.00 | 68.50 | 12.10 | 23257.30 |
| 304 SS (NaOH) | 0.32 | 0.01 | 1.49 | 0.02 | 0.01 | 1.37 | 1.54 | 0.07 | 4.39 | - | - | - | 0.03 | 0.01 | 0.22 |
| CoCrNi (NaOH) | 4.97 | - | 1908.74 | - | - | - | - | - | - | 0.43 | - | 49.83 | 0.55 | - | 37.82 |

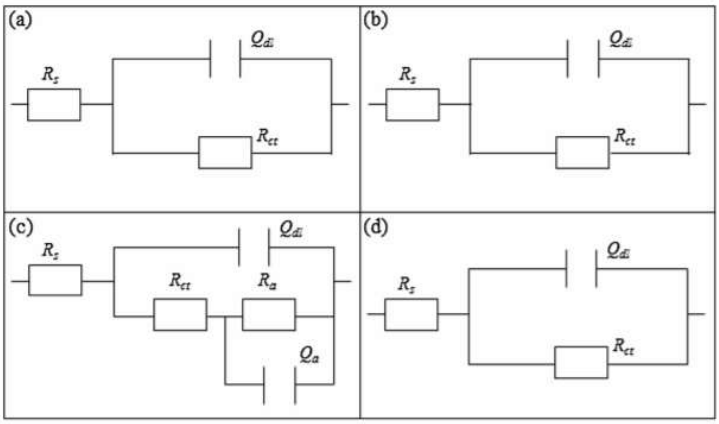


**Fig. 4.** Equivalent electron circuits model for fitting the EIS experimental data; (a) the CoCrNi in $H_2SO_4$ solution; (b) the 304 SS in $H_2SO_4$ solution; (c) the CoCrNi in NaOH solution; (d) the 304 SS in NaOH solution.

On the basis of that, the equivalent electrical circuits for the CoCrNi and the 304 SS in 1.5 M $H_2SO_4$ and 1.5 M NaOH solutions are shown in Fig. 4, in which $R_s$ represents solution resistance, $R_{ct}$ is charge transfer resistance, $R_a$ and $Q_a$ represent the

equivalent resistance and capacitance related to the adsorption process, and $Q_{dl}$ is a constant phase element (CPE) which used to represent the double-layer capacitance and fit the EIS data better since it takes the dispersion behavior into account [38-41]. According to the equivalent electrical circuits, all the EIS data are well fitted, and the detail impedance data are displayed in Table 3. The whole polarization resistance $R_p$ is used to compare the corrosion resistance and it can be calculated with the following equation:

$$R_p = R_s + R_t + R_a \tag{3-1}$$

Obviously, the $R_p$ of CoCrNi is much larger than that of the 304 SS in $H_2SO_4$ solution but opposite in NaOH solution, which also confirms the aforementioned conclusions. The difference in corrosion resistance is caused by the passive film on the sample surface and it will be confirmed by the subsequent XPS and SEM results.

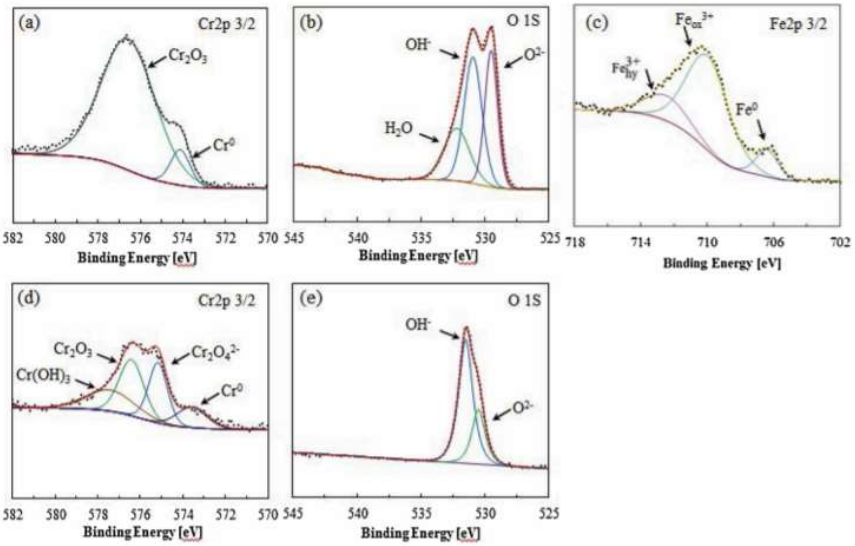


**Fig. 5.** High resolution XPS spectra of the passive films formed on the CoCrNi (a)–(b) and the 304 SS (c)–(e) after passivation in $H_2SO_4$ solution at room temperature. (a), (d) Cr2p 3/2; (b), (e) O 1s; (c) Fe2p 3/2.

Fig. 5 shows the XPS results of Cr $2p_{3/2}$, Fe $2p_{3/2}$, O 1s for the passive film formed on the CoCrNi and the 304 SS after passivation in 1 M $H_2SO_4$ solution. XPS spectra of the Co $2p_{3/2}$ and Ni $2p_{3/2}$ are not given here, for the response is weak and their high-resolution spectra are hard to analyze by fitting the spectra. For the CoCrNi, the Cr $2p_{3/2}$ ionization is divided into two constituent peaks (Fig. 5a), the metallic state $Cr_{(met)}$ (574.1 eV) and $Cr_2O_3$ (576.3 eV). The intensity of $Cr_2O_3$ is much stronger than that of Cr, suggesting that the $Cr_2O_3$ is the primary constituent in the passive film of

the CoCrNi. The O 1s spectra is split into three peaks, the $OH^-$ species (530.8 eV), $O^{2-}$ (529.5 eV) species and a small percentage of $H_2O$ species (532.8 eV). The bound

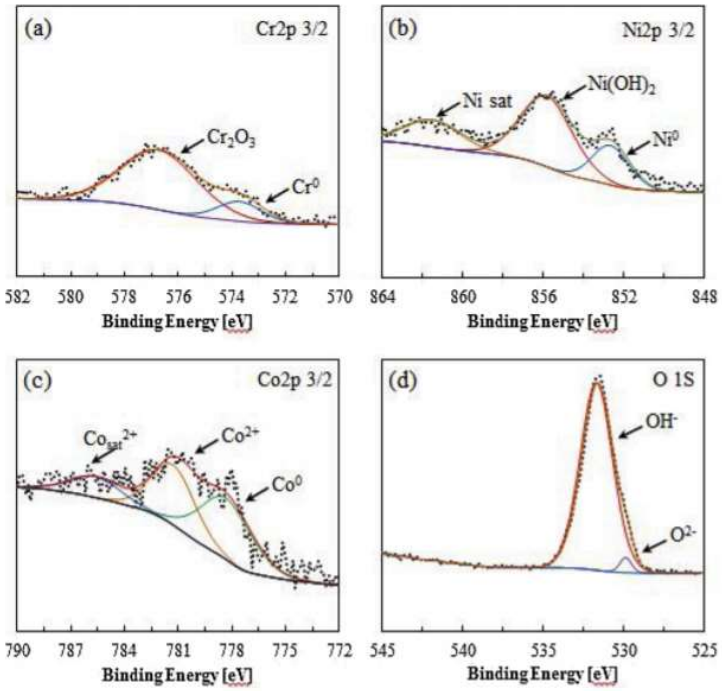


**Fig. 6.** High resolution XPS spectra of the corrosion products formed on the CoCrNi (a)–(d) after passivation in NaOH solution at room temperature. (a) Cr2p 3/2; (b) Ni2p 3/2; (c) Co2p 3/2; (d) O 1s.

water can act as an effective species to capture the dissolving metal ions, forming a new film resisting further corrosive attack [42,43]. In the case of the 304 SS, the valence state of Cr is more complex and it is separated into four peaks which represent the metallic state $Cr_{(met)}$ (573.7 eV), $Cr_2O_4^{2-}$ (574.9 eV), $Cr_2O_3$ (576.3 eV) and $Cr(OH)_3$ (577.3 eV)，respectively. Unlike to the CoCrNi, the primary constituents in the passive film of the 304 SS are the $Cr_2O_4^{2-}$ and $Cr_2O_3$. In addition, three peaks are identified in the Fe $2p_{3/2}$ spectra, i.e., the metallic Fe (706.8 eV), $Fe_{ox}^{3+}$ (709.9 eV), and $Fe_{hy}^{3+}$ (711.8 eV), in which the $Fe^{3+}$ (oxide species) is the primary iron oxidized species in the passive film of the 304 SS. However, the peak pertaining to $H_2O$ in the passive film is absent, which is similar to the case of hydrogen charged passive films observed on duplex stainless steel [44]. Moreover, it can be observed that the $OH^-$ species are the main constituent of the passive film formed on the CoCrNi. From the data above, it can be concluded that Cr oxides play an important role in passive film to protect the inner alloy from corrosion. The deconvolution results of species of all elements indicate that the Cr oxides is the main constituent in the passive film of the CoCrNi, and the Fe and Cr oxide species prevail in the passive film of the 304 SS.

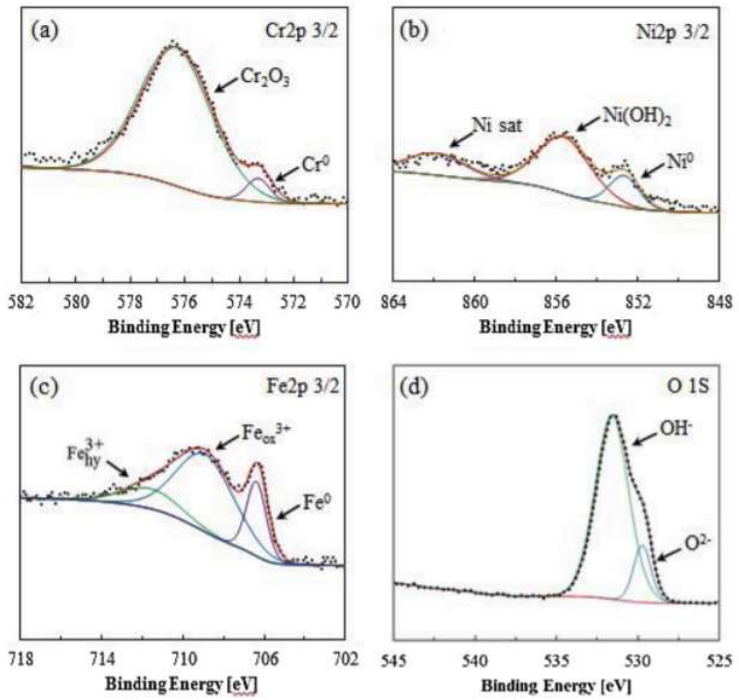


**Fig. 7.** High resolution XPS spectra of the passive films formed on the 304 SS (a)–(d) after passivation in NaOH solution at room temperature. (a) Cr2p 3/2; (b) Ni2 3/2; (c) Fe2p 3/2; (d) O 1s.

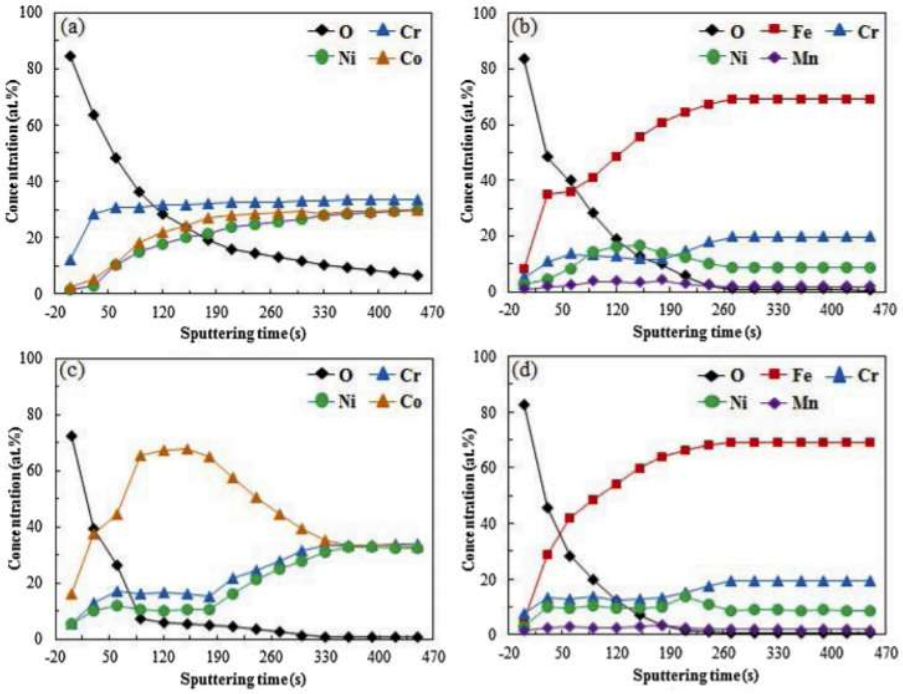


**Fig. 8.** XPS sputtering depth profiles of the alloy elements in the passive films of the CoCrNi and the 304 SS after immersion in $H_2SO_4$ solution (a and b) and I solution (c and d).

Figs. 6 and 7 show the Cr $2p_{3/2}$, Fe $2p_{3/2}$, Ni $2p_{3/2}$, O 1s, and Co $2p_{3/2}$ for the surface of

the CoCrNi and the 304 SS after test in 1.5 M NaOH solutions, respectively. The Cr, Ni, and O elements of the CoCrNi and the 304 SS exhibit similar valence state. The Cr 2p3/2 ionization is split into two peaks which correspond to the metallic state Cr and $Cr_2O_3$. The lower Cr and Cr oxides content of the CoCrNi indicates a large amount of dissolution of Cr in NaOH solution further. The Ni $2p_{3/2}$ spectra are separated into three peaks, associating with the metallic state Ni (852.8 eV), $Ni(OH)_2$ (855.8 eV), and $Ni_{sat}$ (861.9 eV). Previous literatures [30,45,46] have shown that the nickel is less readily oxidized and the metallic Ni is enriched in the oxide/metal interface. Therefore, the Ni and its oxide states are hard to detect in the passive film of austenitic stainless steel. In this work, XPS easily detects Ni because of the high-nickel content in the CoCrNi and no passivation behavior in NaOH solution. The O 1s spectra are split into two peaks, the $OH^-$ species and a small percentage of $O^{2-}$ species correspond to the presence of hydroxide and oxide on the surface of alloys. Besides, three constituent peaks representing the metallic Co, $Co^{2+}$ and $Co^{2+}_{sat}$ are observed in the spectra of Co $2p_{3/2}$ of the CoCrNi. The $Co^{2+}$ satellite peaks are attributable to monopole charge-transfer transitions [47]. The $Co^{2+}$ species are composed of Co-oxide, Co-hydroxide, and their mixtures. Moreover, the metallic Co and $Co^{2+}$ are the primary cobalt species. Similar to the 304 SS in $H_2SO_4$ solution, the metallic Fe, $Fe_{ox}^{3+}$, and $Fe_{hy}^{3+}$ are observed from the Fe $2p_{3/2}$ ionisation. The relative heights of Fe, $Fe_{ox}^{3+}$, and $Fe_{hy}^{3+}$ demonstrate that Fe and $Fe_{ox}^{3+}$ are the primary oxidized species.

Furthermore, XPS depth profiles of main elements in the passive film/corrosion products formed on the CoCrNi and the 304 SS in 1 M $H_2SO_4$ and 1.5 M NaOH solutions are shown in Fig. 8. Obviously, metal elements increase and O element decrease with the increase of sputtering time, suggesting that metal element dissolved and oxide films formed on the surface of the alloys when the corrosion occurred. In $H_2SO_4$ solution, the Cr content on CoCrNi surface is much higher than Ni and Co at the initial stage of sputtering, indicating the selective dissolution of Co and Ni elements occurred and the $Cr_2O_3$ is the main component of the passive film on the CoCrNi further. In the case of the 304 SS in $H_2SO_4$ solution, the entire passive film is enriched in Fe and Cr, and there is a strong enrichment of Ni close to the film/metal interface where Cr is depleted. It is known from the previous analysis that the CoCrNi exhibited superior corrosion resistance than the 304 SS in $H_2SO_4$. It is attributed to that the CoCrNi contains more Cr content and then formed more $Cr_2O_3$ oxides on the

surface, which is beneficial to prevent corrosion. Additionally, the passive film formed on the CoCrNi is thicker than that on the 304 SS.

In 1.5 M NaOH solution, there is also obvious selective dissolution of Ni and Cr on the CoCrNi surface. The concentration of Co in the corrosion products is higher than in the bulk matrix and the Cr and Ni dissolved extensively in the oxide/metal interface. As mentioned above, the metallic Co and $Co^{2+}$ are the primary cobalt species. Although the formation of oxide-cobalt next to the metallic surface lead to passivation of cobalt and oxidation film formation [48], but previous studies have shown that pure cobalt has been found to exhibit no transition from active to passive states in alkaline solutions and Cr and Ni are stable in alkaline environments and forms passivating $Cr_2O_3$ and $Ni_2O_3$ layers [49-51]. For the 304 SS, the passive film mainly contains Cr, which is similar to the situation in $H_2SO_4$ solution. The inferior corrosion resistance of the CoCrNi in NaOH solution is caused by higher content and their higher dissolution rates of Ni and Cr.

### 3.3 Morphology of corroded surfaces

Figs. 9 and 10 show the surface morphology of the CoCrNi and the 304 SS after immersion in 1 M $H_2SO_4$ and 1.5 M NaOH solutions at room temperature. In $H_2SO_4$ solution, a large amount of rough corrosion products generated and covered the surface of the CoCrNi in $H_2SO_4$ solution. The EDS results exhibit that the Co and Ni elements are concentrated in areas with less corrosion products, while the Cr and O elements are concentrated in areas with more corrosion products. It indicates that selective dissolution occurred and the Cr oxides are the primary component of the passive film in the further, which is also consistent with ICP and XPS results. In addition, elements are uniformly distributed on the surface of the 304 SS. The nano-sized pores on the surface of the 304 SS suggest that it suffered from pitting corrosion, which lead to its inferior corrosion resistance in $H_2SO_4$ solution. In NaOH solution, many corrosion pores and obvious intergranular corrosion appeared on the CoCrNi surface. Unlike the situation in $H_2SO_4$ solution, Cr and O elements are uneven distributed and concentrated in the corrosion area, resulting in less oxides covered the surface and poor corrosion resistance. On the contrary, the 304 SS surface is relatively smoother and it appears to have superior corrosion resistance with slight pitting corrosion. This phenomenon can be attributed to the oxides which are uniformly distributed on the surface of the 304 SS and protect the alloy from the

corrosion.

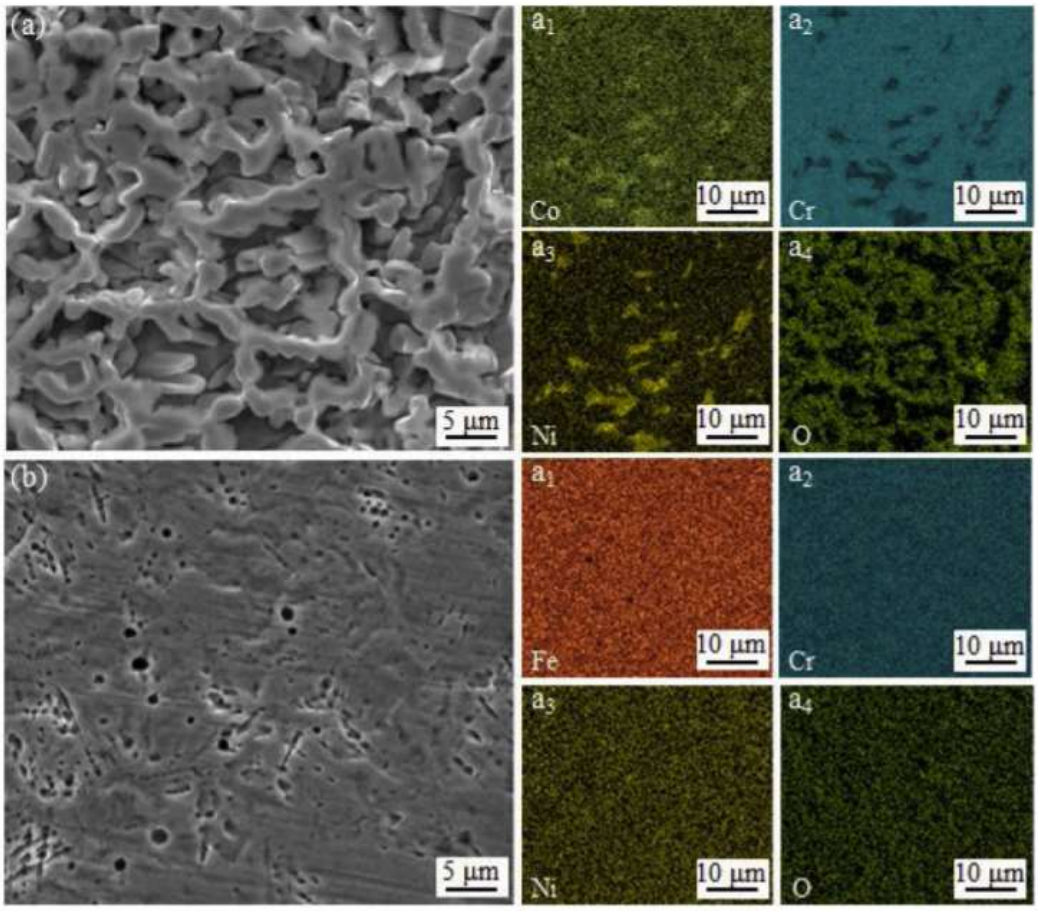


**Fig. 9.** EDS mapping of the equiatomic CoCrNi (a) and the 304 SS (b) after immersion in $H_2SO_4$ solution.

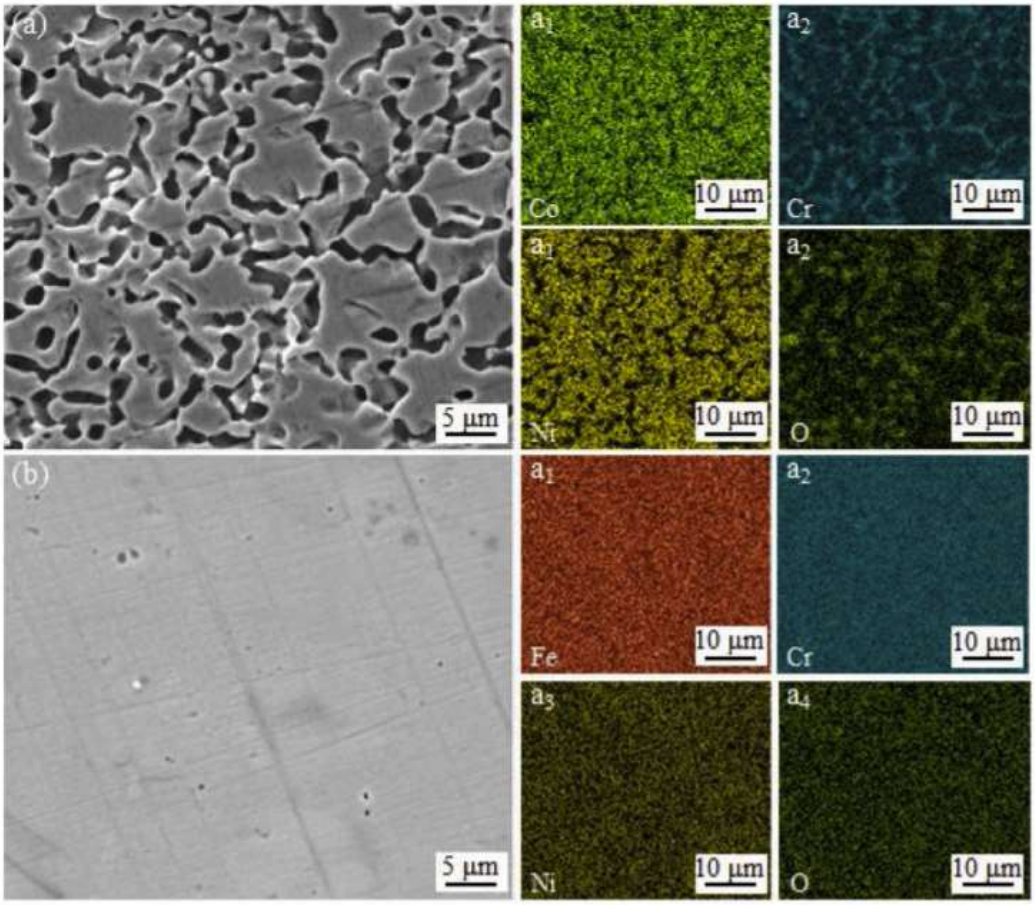


**Fig. 10.** EDS mapping of the equiatomic CoCrNi (a) and the 304 SS (b) after immersion in NaOH solution.

Based on the above descriptions and discussions, the corrosion processes of the CoCrNi and the 304 SS in 1 M $H_2SO_4$ and 1.5 M NaOH solutions are schematically described in Fig. 11. Several previous studies have demonstrated that the corrosion resistance of metallic alloys is highly dependent on the composition and structure of the passive films formed in the solution [30,52,53]. In the present work, the excellent corrosion resistance of the CoCrNi in $H_2SO_4$ can also be ascribed to the stable passive film exposing to the environment. As shown in Fig. 11, compared with the 304 SS in $H_2SO_4$ solution, the passive film without pitting corrosion of the CoCrNi is thicker. As described earlier, the main composition of the passive film on the 304 SS is the Fe and Cr oxides. In the case of the CoCrNi, the high concentration of Cr could in principle be expected to be also beneficial for the materials' corrosion resistance. The corrosion resistance of the CoCrNi is higher than that of the 304 SS since its passive film formed in 1 M $H_2SO_4$ is more stable, thick and without pitting corrosion. In addition, for the corrosion resistance of the CoCrNi and the 304 SS in NaOH solution, the passivation did not observe on the CoCrNi and a large amount of dissolution of the Cr

element in the solution, which resulting in obvious pores and serious intergranular corrosion. In the case of the 304 SS, the stable and thicker passive film results in higher corrosion resistance in NaOH solution.

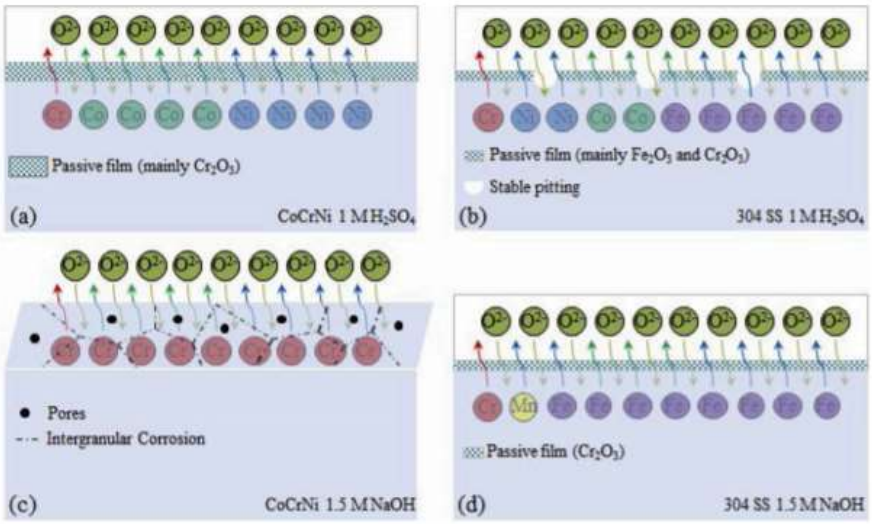


**Fig. 11.** Schematic diagram of corrosion processes of the CoCrNi (a and c) and the 304 SS (b and d) in $H_2SO_4$ and NaOH solutions.

## 4. Conclusion

The corrosion behavior and composition of the passive films of the CoCrNi medium-entropy alloy (MEA) and the 304 SS in 1 M $H_2SO_4$ and 1.5 M $H_2SO_4$ solutions were investigated in detail by XPS and ICP methods. The main conclusions are:

1. The CoCrNi exhibits superior corrosion resistance in $H_2SO_4$ solution while shows inferior corrosion resistance in NaOH solution compared with the 304 SS.
2. The CoCrNi shows passive behavior in 1 M $H_2SO_4$ solution, but not find in 1.5 M NaOH solution.
3. In 1 M $H_2SO_4$ solution, the main constituent of the passive film on the CoCrNi is Co oxides, while the passive film on the 304 SS shows as main components hydroxides of Fe mixed with Cr oxides. The corrosion resistance of the CoCrNi is higher since its passive film is more stable, thick and without pitting corrosion.
4. In 1.5 NaOH solution, a large amount of dissolution of Cr element occurs in the solution, which resulting in obvious pores and serious intergranular corrosion. In the case of the 304 SS, the stable and thicker passive film results in higher corrosion

resistance.

**Acknowledgments**

This project was financially supported by National Natural Science Foundation of China with No. 51404302.

**References**

[1] J.W. Yeh, S.K. Chen, S.J. Lin, J.Y. Gan, T.S. Chin, T.T. Shun, C.H. Tsau, S.Y. Chang, Adv. Eng. Mater. 6 (2004) 299–303.

[2] B. Cantor, I.T.H. Chang, P. Knight, A.J.B. Vincent, Mater. Sci. Eng.: A 375 (2004) 213–218.

[3] B. Gludovatz, A. Hohenwarter, K.V.S. Thurston, H.B. Bei, Z.G. Wu, E.P. George, Nat Commun. 7 (2016) 10602.

[4] J.Y. Wang, H.L. Yang, H. Huang, J.M. Ruan, S.X. Ji, J. Alloys. Comp. 798 (2019) 576–586.

[5] B. Cantor, Entropy 16 (2014) 4749–4768.

[6] Y.L. Zhao, T. Yang, Y. Tong, J. Wang, J.H. Luan, Acta Mater. 138 (2017) 72–82.

[7] Y. Ma, F. Yuan, M. Yang, P. Jiang, E. Ma, Acta Mater. 148 (2018) 407–418.

[8] S. Yoshida, T. Bhattacharjee, B. Yu, N. Tsuji, Scripta Mater. 134 (2017) 33–36.

[9] J.Y. Wang, H.L. Yang, Z.L. Liu, S.X. Ji, R.D. Li, J.M. Ruan, J. Alloys Comp. 772 (2019) 272–279.

[10] V.T. Nguyen, M. Qian, Z. Shi, T. Song, L. Huang, J. Zou, Intermetallics. 101 (2018) 39–43.

[11] C. Zhang, Y. Wu, L. You, X.Z. Cao, X.P. Song, J. Alloys Comp. 781 (2019) 613–620.

[12] S.P. Wang, E. Ma, J. Xu, Intermetallics. 103 (2018) 78–87.

[13] Z. Wu, H. Bei, F. Otto, G. Pharr, E.P. George, Intermetallics. 46 (2014) 131–140.

[14] H. Luo, Z.M. Li, A.M. Mingers, D. Raabe, Corros. Sci. 134 (2018) 131–139.

[15] Y.Z. Shi, B. Yang, X. Xie, J. Brechtl, K.A. Dahmen, Corros. Sci. 119 (2017) 33–45.

[16] X.L. Niu, L.J. Wang, D. Sun, J. Julius, J. Funct. Mater. 4 (2013) 532–535.

[17] H. Feng, H.B. Li, X.L. Wu, Z.H. Jiang, S. Zhao, J. Mater. Sci. Technol. 34 (2018) 1781–1790.

[18] Y.J. Hsu, W.C. Chiang, J.K. Wu, Mater. Chem. Phys. 92 (2005) 112–117.

[19] Y.C. Cai, Y. Chen, Z. Luo, F. Gao, Lun, Li, Mater. Des. 133 (2017) 91–108.
[20] I. Moravcik, J. Cizek, Z. Kovacova, J. Nejezchlebova, M. Kizmantel, Mater Sci Eng A. 119 (2017) 33–45.
[21] S. Ma, S. Zhang, J. Qiao, Z. Wang, M. Gao, Z. Jiao, H. Yang, Y. Zhang, Intermetallics 54 (2014) 104–109.
[22] A.D. Schino, J.M. Kenny, J. Mater. Sci. Lett. 21 (2002) 1631–1634.
[23] K. Ralston, N. Birbilis, Corrosion 66 (2010) (075005-075005-075013).
[24] K.S. Raja, S.A. Namjoshi, M. Misra, Mater. Lett. 59 (2005) 570–574.
[25] X.Y. Wang, D.Y. Li, Electrochim. Acta 47 (2002) 3939–3947.
[26] X.W. Qiu, Y.P. Zhang, L. He, C.G. Liu, J. Alloys Compd. 549 (2013) 195–199.
[27] X.W. Qiu, Y.P. Zhang, C.G. Liu, J. Alloys Compd. 585 (2014) 282–286.
[28] S. Pengaraju, L. Neelakantan, R.G. Pillai, Electrochim. Acta 308 (2019) 131–141.
[29] S.H. Chang, L.Y. Hung, T.H. Yang, Mater Chem Phys. 235 (2019) 121743.
[30] C.O.A. Olsson, D. Landolt, Electrochim .Acta 48 (2003) 1093–1104.
[31] J. Castle, J. Qiu, Corros. Sci. 29 (1989) 591–603.
[32] D. Hamm, K. Ogle, C.O. Olsson, S. Weber, D. Landolt, Corros. Sci. 44 (2002) 1443–1456.
[33] S. Haupt, H.H. Strehblow, J. Electroanal. Chem. Interfacial Electrochem. 216 (1987) 229–240.
[34] Y. Zhang, J. Wu, X. Yu, H. Wu, Appl. Surf. Sci. 257 (2011) 7928–7931.
[35] A. Nishikata, Y. Ichihara, T. Tsuru, Electrochim. Acta. 41 (1996) 1057–1062.
[36] C.N. Cao, Electrochim. Acta, 35 (1990) 831–836
[37] H. Luo, S. Gao, C. Dong, X. Li, Electrochim. Acta, 135 (2014) 412–419.
[38] B. Rosborg, T. Kosec, A. Kranjc, J. Pan, A. Legat, Electrochim. Acta, 56 (2011) 7862–7870.
[39] R.N. Deo, N. Birbilis, J.P. Cull, Corros. Sci. 80 (2014) 339–349.
[40] Z. Cui, L. Wang, H. Ni, W. Hao, C. Man, S. Chen, X. Wang, Z. Liu, X. Li Corros. Sci. 118 (2017) 31–48.
[41] Y. Wang, Y. Qiu, Z. Chen, X. Guo, Corros. Sci. 118 (2017) 96–108.
[42] G. Okamoto, Corros. Sci. 13 (1973) 471–489.
[43] G. Okamoto, T. Shibata, Nature, 206 (1965) 1350.
[44] G. Okamoto, Corros. Sci. 13 (1973) 471–489.

[45] M.J. Carmezim, A.M. Simões, M.F. Montemor, M.D. Cunha Belo, Corros. Sci. 47 (2005) 581–591.
[46] A. Kocijan, Č. Donik, M. Jenko, Corros. Sci. 49 (2007) 2083–2098.
[47] T. Chuang, C. Brundle, D. Rice, Surf. Sci. 59 (1976) 413–429.
[48] T. Jayaraman, V. Venkatesan, H. Udupa, Electrochim. Acta, 20 (1975) 209–213.
[49] F.J.J Kellner, M.S. Killian, G. Yang, E. Spiecker, S. Virtanen, Int. J. Refract. Met. Hard Mater. 29 (2011) 376–383.
[50] W. Tang, L. Zhang, Y. Chen, H.D. Zhang, L. Zhou, Int. J. Refract. Met. Hard Mater. 68 (2017) 1–8.
[51] X. Zhang, J.H. Zhou, C. Liu, K. Li, W.J. Shen, Int. J. Refract. Met. Hard Mater. 80 (2019) 123–129.
[52] G. Burstein, P. Marshall, Corros. Sci. 23 (1983) 125–137.
[53] G. Ilevbare, G. Burstein, Corros. Sci. 43 (2001) 485–513.